RESEARCH ARTICLE

Practical limits of multijunction solar cells

Ian Marius Peters[1] | Carlos David Rodríguez Gallegos[2] | Larry Lüer[3] |
Jens A. Hauch[1,3] | Christoph J. Brabec[1,3]

[1]Forschungszentrum Jülich, Helmholtz Institute Erlangen-Nürnberg for Renewable Energies HI ERN, Erlangen, Germany

[2]Solar Energy Research Institute of Singapore (SERIS), National University of Singapore (NUS), Singapore

[3]Institute Materials for Electronics and Energy Technology i-MEET, Friedrich Alexander University (FAU), Erlangen, Germany

Correspondence
Ian Marius Peters, Forschungszentrum Jülich, Helmholtz Institute Erlangen-Nürnberg for Renewable Energies HI ERN, Immerwahrstraße 2, Erlangen, Germany.
Email: im.peters@fz-juelich.de

Abstract

Multijunction solar cells offer a path to very high conversion efficiency, exceeding 60% in theory. Under ideal conditions, efficiency increases monotonically with the number of junctions. In this study, we explore technical and economic mechanisms acting on tandem solar cells. We find that these mechanisms produce limitations that are the more pronounced the greater the number of junction is and, hence, limit the ideal number of junctions, as well as the corresponding efficiencies. Spectral variations induce current losses in series-connected tandem solar cells. For Denver, we find that these losses reduce achievable harvesting efficiencies to 51% for non-concentrated light and that they restrict the ideal number of junctions to less than nine. Independently operated solar cells suffer from optical losses with similar consequences. Even high optical efficiencies of 99% restrict the ideal number of junctions to below 10 and reduce achievable efficiencies by more than 10%. Only architectures with a sequential cell illumination are more resilient to these losses. Restricting available materials reveals that a sufficiently low band gap for the bottom cell of 0.9 eV or below is expedient to realize high efficiencies. Economic considerations show that five junctions or less are economically ideal for most conceivable applications.

KEYWORDS
multijunction solar cell, solar spectrum, techno-economic modelling

1 | INTRODUCTION

Multijunction solar cells, in the following also referred to as tandems, combine absorbers with different band gaps to reduce two principle loss mechanisms occurring in single junction solar cells: thermalization and sub-band gap losses.[1] Increasing the number of junctions towards infinity monotonically increases the detailed balance efficiency limit to more than 65% without concentration and more than 85% with concentration[2]—about twice the limit of a single junction solar cell.[3] Yet, these values are obtained from calculations that use very few constraints. Neither optics nor interconnections are considered, the solar cells are illuminated with one unwavering spectrum at one given intensity and they operate at

one set temperature. Such conditions can be approached in the lab, with some effort, but they cannot be realized in the field. Introducing constraints results in the formation of losses, and these losses, for fundamental reasons, affect tandems with different numbers of junctions differently. In this study, we explore a few of these constraints, and we show that they result in the formation of a finite optimum number of junctions exhibiting the greatest limiting efficiency. For the definition of the included constraints, it is useful to distinguish between different architectures of tandem solar cells and different interconnection schemes. In the next section, we introduce four different tandem architectures. We then explore limiting efficiencies without and with constraints due to available materials, variation in spectrum and imperfect optics. In a final investigation, we

explore economic constraints using a simple bottom-up cost model for a perovskite-based multijunction solar cell.

2 | TANDEM ARCHITECTURES

In this study, we distinguish four types of tandem architectures based on the optical mechanism used for spectral splitting. For each architecture, there are several possibilities of electrical integration, which we will discuss later. The four architectures are displayed in Figure 1. The first architecture (Figure 1A) is termed stacking. In this architecture, cells are stacked on top of each other in order of decreasing band gap. Spectral splitting is achieved via selective absorption in the semiconductor absorbers; no additional optical components are required. This architecture is the most commonly realized tandem with achieved efficiencies of above 47%[4,5] under concentration and

above 39%[4,6] without concentration. The second architecture is termed optical splitting (Figure 1B). In this architecture, spectral selection is achieved via an optical element like a grating,[7,8] a prism[9] or a holographic element.[10,11] The optical element splits white light spatially into different wavelengths. Cells can be placed underneath such that each cell receives the part of the spectrum most suitable for it. The use of an optical element allows decoupling the aperture area from the cell area, which can be used for concentration or de-concentration. The highest efficiency reported for this configuration is 42.7%[9] for separately operated solar cells. A variation of this concept is the stacked fluorescent concentrator,[12] in which light is split by selective absorption and emission and is spatially separated via total internal reflection.

The third architecture utilizes spatial randomization and spectral selection via filters, and it is termed randomized spectral selection (Figure 1C). Light falls through a small aperture into a body covered
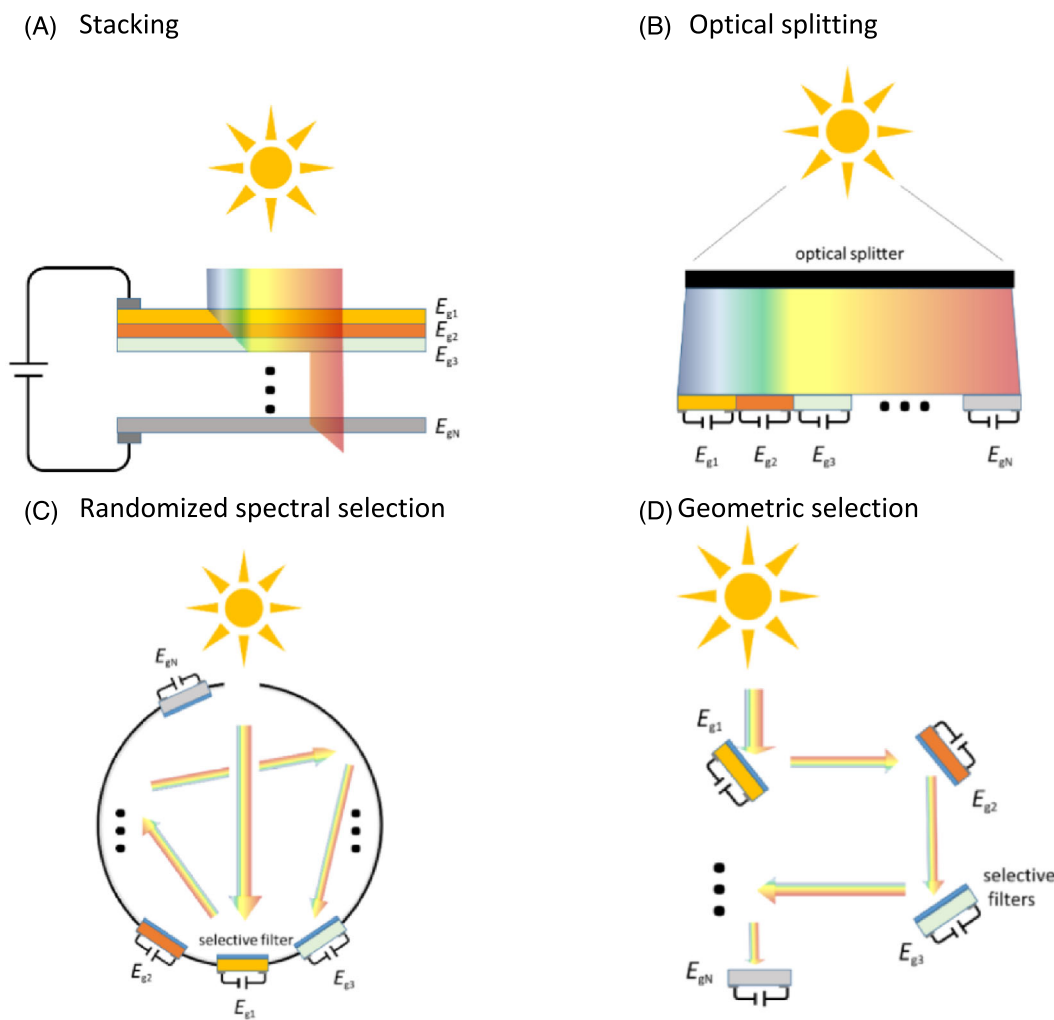

FIGURE 1 Different tandem architectures. (A) Cells with decreasing band gaps are stacked on top of each other. Each cell acts as a filter for subsequent cells and absorbs the part of the spectrum in which it is optically active. (B) Cells are arranged sequentially, typically ordered by band gap. An optical element splits the spectrum such that each cell is illuminated with the part of the spectrum in which it is active. (C) Cells are equipped with selective filters that are transmitting the spectral range in which the cell is active and reflect all other light. Cells are arranged such that light reaches each cell after a series of scattering and reflection events. (D) Cells are equipped with selective filters but are arranged geometrically that light is guided from one cell to the next.
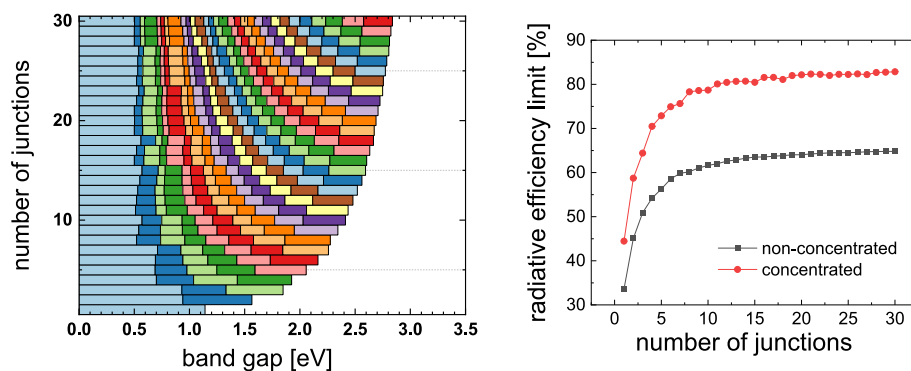
FIGURE 2 Left: Ideal band gaps calculated for the AM1.5d spectrum under concentrated light. Coloured ranges are shown for visualization purposes. The discrete band gap values are located at the intersection between colours. Right: Corresponding limiting efficiencies for concentrated- (red) and nonconcentrated light (black) calculated for the AM1.5g and AM1.5d spectrum, respectively.

with a highly reflective scattering surface. Spectral selection is achieved via band pass filters that only transmit light intended for a particular solar cell. Solar cells and filter are placed on the inner sidewalls of the body. Light reaches all cells after a sequence of scattering and reflecting events. The size of the solar cells determines the concentration/deconcentration factor of the setup. With this setup, efficiencies of 14.2% were reported for silicon solar cells and illumination with a high power laser.[13] Geometric selection (Figure 1D), finally, utilizes a geometric arrangement in which light is guided towards various solar cells via directed reflection. Spectral selection, like in the previous concept, is achieved by placing selective filters in front of every solar cell but the last. The highest efficiency achieved with this setup is 34.3%, measured outdoors.[14]

All architectures permit a series connection of all cells (2-terminal setup), individually contacting each cell (2N-terminal setup), or a combination of these. Only in the stacking architecture can cells be monolithically integrated. Series connection entails a current matching requirement—the cell with the lowest current limits the current of the entire stack. All architectures also permit the integration of concentration or deconcentration using the available (architectures *b* and *c*) or additional (architectures *a* and *d*) optical elements like lenses.

3 | BAND GAPS AND LIMIT UNDER AM1.5 SPECTRUM

Thermalization and sub-band gap transmission limit the efficiency of a solar cell.[1] Tandems expand the spectral absorption range compared to a single-junction solar cell by integrating materials with a lower band gap. In radiative limit calculations, absorbers are treated as grey bodies[15]; hence, the material with the lowest band gap determines the lowest photon energy that can still be utilized—photons with greater energy are absorbed with a probability of one. Thermalization is the process of cooling the electron gas in the semiconductor from the temperature of the sun to ambient. Free electrons can be utilized with an energy equal to the quasi-Fermi level difference at the terminals of the semiconductor. In an efficient solar cell, this difference is determined predominantly by the band gap energy E_g of the semiconductor. Introducing additional junctions with greater band gap energies results, hence, in a more efficient utilization on the sunlight's

energy. The band gap combination yielding the greatest efficiency depends on the shape of the illumination spectrum. Figure 2 shows the band gap combinations and for up to 30 junctions and the maximum efficiency, calculated using the detailed balance approach[16] for the AM1.5 solar spectrum,[17] with no (AM1.5g)- and maximum concentration (AM1.5d). Concentrating light reduces the entropic loss associated to Étendue[18] and results in a principally higher voltage of solar cells. Due to numerical variations in input data and optimization procedures, there are small variations possible; the present calculations find that the efficiency for concentrated light converges towards 83% and 65% for non-concentrated light in the limit of an infinite tandem. De Vos[2] quotes values of 86% and 68%; note that the incident spectrum in his case was blackbody radiation at 6000 K.

4 | EFFICIENCY LIMITS WITH BAND GAP CONSTRAINTS

A first limitation explored here concerns the availability of materials with suitable band gaps. In practice, the range of band gaps that can be used for tandem solar cells will be restricted, either for fundamental or for practical reasons. One example for such restrictions are III-V materials. In a lattice-matched configuration, using a germanium substrate and GaAs, AlAs combinations, a band gap range between 0.6 eV and 2.12 eV is available. This range can be expanded by adopting a technique referred to as lattice-mismatched-[19,20] or metamorphic[19] growth, or by direct wafer bonding.[21] InAs has a band gap of 0.36 eV and AlP one of 2.45 eV. Even higher band gaps are in principle available (GaN, for example, goes to 3.4 eV, although at a different crystal structure). Band gap information was taken from Bett et al.[22] Perovskite materials also permit varying band gaps by substitution of halides and cations. The near-surface band gap of methyl-ammonium-lead-iodide ($MaPbI_3$) was measured at 1.59 eV.[23] Replacing iodine with bromine increases the band gap up to 2.3 eV.[24] Variation of the A-site cation in the lead- and tin-based perovskite $FA_{1-x}Cs_xMI_3$ (M = Sn, Pb) allows reducing the band gap down to 1.24 eV.[25] In practice, creating materials with targeted band gaps may face additional challenges such as certain III-V materials becoming indirect semiconductors or perovskites featuring low phase stability.

FIGURE 3 Efficiency limit for a multijunction solar cell with three to six junctions, if the lowest available band gap is given by the value on the x-axis and the highest band gap is given by the value on the y-axis.
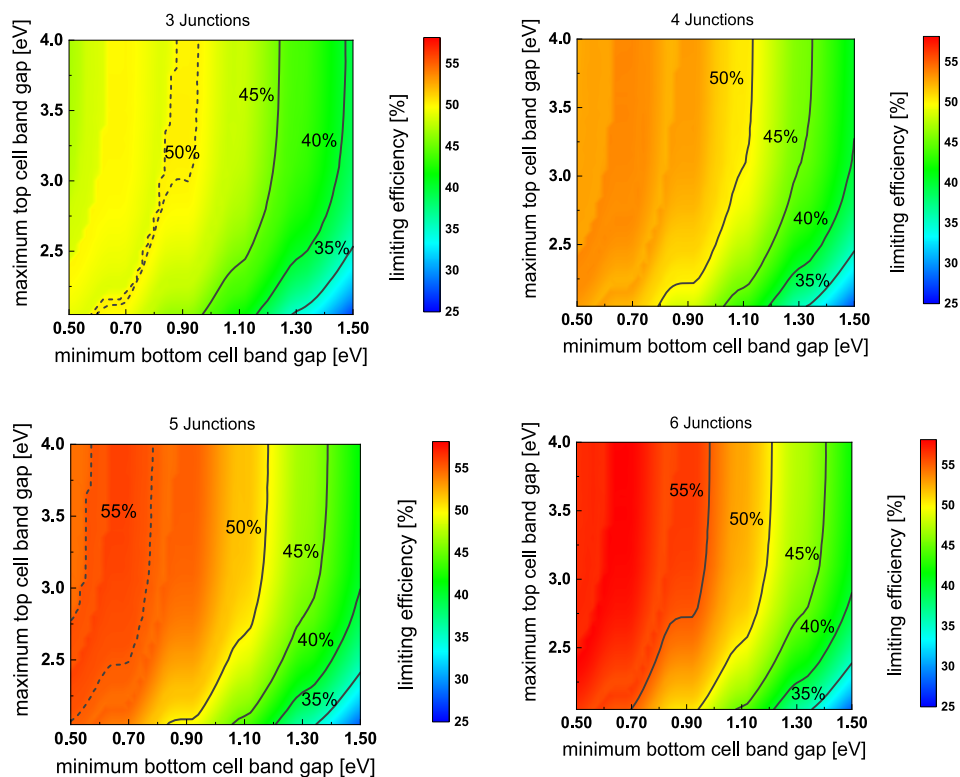

Figure 3 shows a detailed balance efficiency calculation for tandem solar cells with between three and six junctions in which the greatest and the smallest band gap are fixed to the values at the x- and y-axes. The top cell band gap is varied between 2.0 eV and 4.0 eV and the bottom cell band gap between 0.5 eV and 1.5 eV. We observe that in this range, the availability of a suitably low band gap for the bottom cell is more significant than having a high band gap for the top cell. For example, a detailed balance limit above 50% with less than six junctions is only possible, if a lower band gap of 0.9 eV or less is available. For the band gap of the top cell, even a band gap of 2 eV is sufficient to approach the efficiency limit closely in all cases, though it requires a very small band gap of the bottom cell. Band gaps above 2.5 eV reduce the sensitivity of efficiency to the bottom cell band gap notably. If materials can be chosen with band gaps between 0.9 eV (bottom cell) and 2.5 eV (top cell), the limiting efficiencies for three to six junctions are 48.8% (97% of the limit), 51.2% (96%), 52.8% (94%) and 54.0% (93%), respectively.

5 | SERIES CONNECTION AND SPECTRAL VARIATIONS

As mentioned, all tandem architectures shown in Figure 1 can be realized with a series connection of the used cells, either through circuit interconnection or through monolithic integration. Series connection entails a current limitation and design of a series connected tandem will aim for current matching to maximize efficiency. In outdoor operation, the spectrum changes over the course of a day and with seasons[26] due to variations of air mass, atmospheric composition and albedo scattering.[27] The list of papers discussing spectral effects for tandem (and single junction) solar cells is too long for this bibliography. A few noteworthy papers are provided.[28–47] Deviations from the design spectrum, typically AM1.5g, result in some junctions producing greater currents and other junctions producing smaller currents. The greater the number of junctions, the higher the probability that one junction will produce a significantly lower current than under reference conditions and will, hence, reduce the efficiency of the tandem. Spectral impacts on multijunction solar cells are well established both theoretically and experimentally.[28–31] We have calculated the limiting harvesting efficiency (i.e., the quotient of yield and total incoming power) for the year 2018 for the band gap combinations shown in Figure 2A using spectra from Singapore[32] and Denver.[33] Spectra were measured once per minute over the entire time the sun was up. Measurements in Singapore cover a spectral range from 300 nm to 1050 nm and in Denver from 280 nm to 1660 nm. Spectra in either location were supplemented with a scaled AM1.5g spectrum for greater wavelengths. Calculations were configured such that junctions absorbing in the range not covered by measurements were not limiting current. Note that this calculation does not include photon coupling between junctions. Depending on luminescent efficiency, position of the limiting junction, and refractive index, photon coupling could noticeably reduce mismatch losses. Calculations also do not include variations in temperature, just spectral effects. A repetition of the calculation for Denver at 350 K for ideal grey body
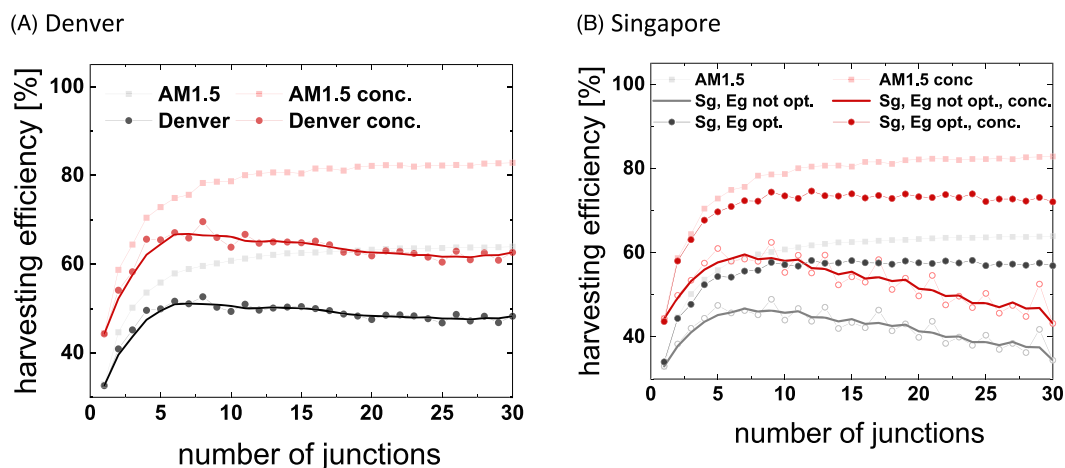
(A) Denver

(B) Singapore

FIGURE 4 Limiting harvesting efficiencies for Denver (A, left) and Singapore (B, right) for concentrated (red) and nonconcentrated (black) light. The calculations for Denver were carried out for then band-gap combination shown in Figure 2A. For Singapore, two calculations were carried out, one for the band gap combination in Figure 2A (solid lines) and one for a band gap combination that was optimized for the spectral conditions in Singapore (dotted lines). More information in Appendix S1.

semiconductors revealed that neither the set of ideal band gaps nor the position of the efficiency maximum changed.

The AM1.5 spectrum does not match average conditions in Singapore well. Consequently, a tandem optimized for this spectrum suffers high mismatch losses that increase with the number of junctions. The mismatch also manifests itself in a strong oscillation as different junction combinations become randomly more or less suited to Singapore conditions. Mismatch losses are reduced if the band gap combination is adjusted to match current generation under the average spectrum in Singapore for the investigated period.[34] This optimization is shown in Figure 4B with dotted lines. Harvesting efficiencies increase, and oscillations reduce. We expect that an adjustment for band gaps in Denver for the predominant spectrum in 2018 would have a similar effect.

For all cases, Denver and Singapore, band gaps optimized or not, mismatch losses increase with the number of junctions. A consequence of these losses is that efficiency no longer increases monotonically with the number of junctions, but converges and even decreases, leading to the formation of a maximum. In Denver, the maximum emerges for eight junctions with harvesting efficiencies of 53% and 70% for concentrated light. In Singapore, the maximum is very flat. After nine junctions, no further significant increase appears, and after 15 junctions, a decrease is notable. Maximum harvesting efficiencies are 58% and 74% for concentrated light.

In the radiative limit, temperature does not affect the ideal combination of band gaps. Physical properties of non-ideal semiconductors, including the band gap, are affected by temperature, though. Hence, temperature variations may result in mismatch losses similar to those caused by spectrum variations and an optimization of band gaps for a particular tandem architecture should consider the operating temperature of the junctions.

6 | INDEPENDENT OPERATION AND OPTICAL EFFICIENCY

Current matching is no concern if cells are operated and contacted individually. Yet, independent operation requires the introduction of optically active elements. For the architectures shown in Figure 1B–D, these elements are the optical splitter and filters. Yet even in the stacking architecture, contacts and a transparent insulating layer are required to separate cells electrically in a 2N-terminal configuration. These optical elements will never work with perfect optical efficiency. Optical losses will affect tandem efficiency and will be greater for tandems with a greater number of junctions. In the following, we discuss how optical losses will affect the different tandem architectures:

6.1 | Splitting

Optical splitting requires an element to distribute the spectrum onto the various solar cells (Figure 1B). The efficiency of this optical element is defined by how accurately the spectrum is distributed spatially, which can be determined by the divergence of the transmitted beam. This divergence will create an error that will affect each junction. Consequently, losses will increase with the number of junctions:

$$\eta_o(N) = 1 - \frac{1}{\frac{1}{(N \cdot (1-\eta_o))} + 1} \tag{1}$$

In this equation, N is the number of junctions, and η_o is the optical efficiency of the element for a single junction application. The impact of optical losses on the limiting efficiency is shown in Figure 5 on the left.
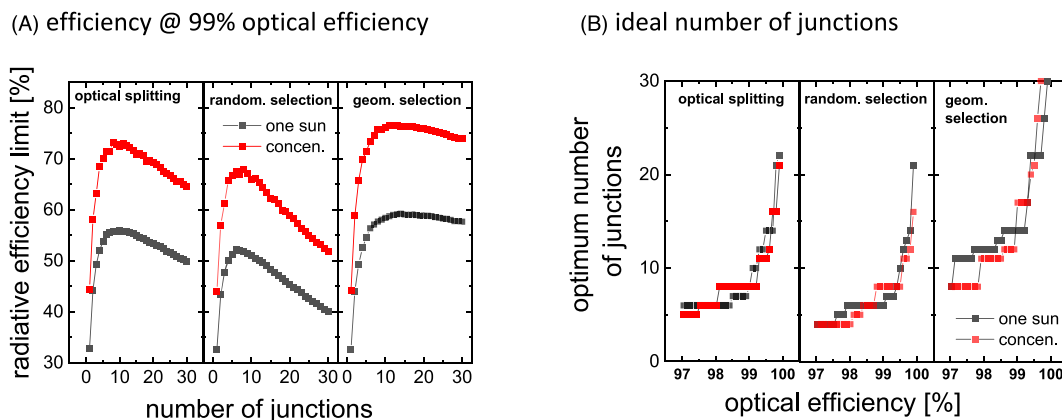
(A) efficiency @ 99% optical efficiency

(B) ideal number of junctions

FIGURE 5 Limiting efficiency for the different configurations with separate cell connections in Figure 1. Figure 5A shows the limiting efficiency for an optical efficiency of 99%, Figure 5B shows the ideal number of junctions as a function of optical efficiency. All shown results utilize the band-gap combination shown in Figure 2A.

6.2 | Randomized spectral selection

In this configuration, there are three contributions to optical efficiency: reflectance of the side walls, unwanted reflectance of the selective filter in the range where it should be translucent and unwanted transmission through the filter were it reflects. For simplicity, we use the same optical efficiency value for all these mechanisms, which could also be viewed as a lumped efficiency. Absorption on the sidewalls reduces light intensity overall; reflection of the filters prevents light from entering the solar cell. The optical efficiency in this configuration is calculated iteratively. In each step holds

$$R_{W,i}(N) = (R_{W,i-1} + R_{C,i-1}) \cdot \left(1 - \frac{A_C}{N \cdot A}\right) \cdot \eta_o \quad (2)$$

$$R_{C,i}(N) = (R_{W,i-1} + R_{C,i-1}) \cdot (1 - \eta_o) \cdot \frac{A_C}{N \cdot A} \quad (3)$$

$$\eta_{C,i}(N) = (R_{W,i-1} + R_{C,i-1}) \cdot \frac{A_C}{N \cdot A} \cdot \eta_o \quad (4)$$

$$\eta_o(N) = \sum_i \eta_{C,i} \quad (5)$$

In these equations, $R_{W,i}$ is the weighted reflectance of the walls during the ith path ($R_{W,0} = 1$), $R_{C,i}$ is the weighted reflectance of the light on the area covered with the targeted cell ($R_{C,0} = 1$) and $\eta_{C,i}$ is the absorptance of light by the targeted on the ith path, A_C is the total area covered with solar cells and A is the total inner surface of the sphere. In the calculated example (Figure 5, centre), half the body is covered with cells ($\frac{A_C}{A} = 0.5$).

6.3 | Geometric selection/stacking

In these configurations (Figure 1A,D), light encounters multiple optical elements or layers on its path to the different solar cells. In the stacking architecture, optical efficiency is determined by the transmission through each junction, in the geometric selection architecture by transmittance and reflectance through the filter. Optical losses increase exponentially as the light beam interacts with more optical elements on its path:

$$\eta_o(N) = \eta_o{}^N \quad (6)$$

Losses are calculated separately for each junction, and efficiencies are summed up in the end. For the geometric selection architecture, it may be possible to reduce losses by realigning band gaps. We have not succeeded in finding a combination that increases the efficiency, though.

Note that in all cases, optical losses affect primarily current, though a reduced current also results in a slight reduction of the produced voltage. This change in voltage was neglected in all calculations and results in a small overestimation of the shown efficiencies. Figure 5A plots the radiative efficiency limit as a function of the number of junctions N for a single-path optical efficiency $\eta_o = 0.99$ for concentrated and non-concentrated light. Figure 5B plots the ideal number of junctions as a function of η_o. Tandems are sensitive to optical losses, especially as the number of junctions goes up. Even an optical efficiency of 99% will result in no further efficiency gains after about seven junctions in the splitting and randomized selection configuration. The geometric selection configuration is less sensitive because optical losses only accumulate at later cells. The ideal number of junctions drops to less than 10, if the optical efficiency is below 97%.

7 | BOTTOM-UP COST MODEL

Yet another limitation for tandem solar cells comes from costs required for their fabrication. The fabrication of a tandem always requires additional steps compared to a single junction solar cell. Exemplarily, this is shown for a double junction perovskite solar cell in
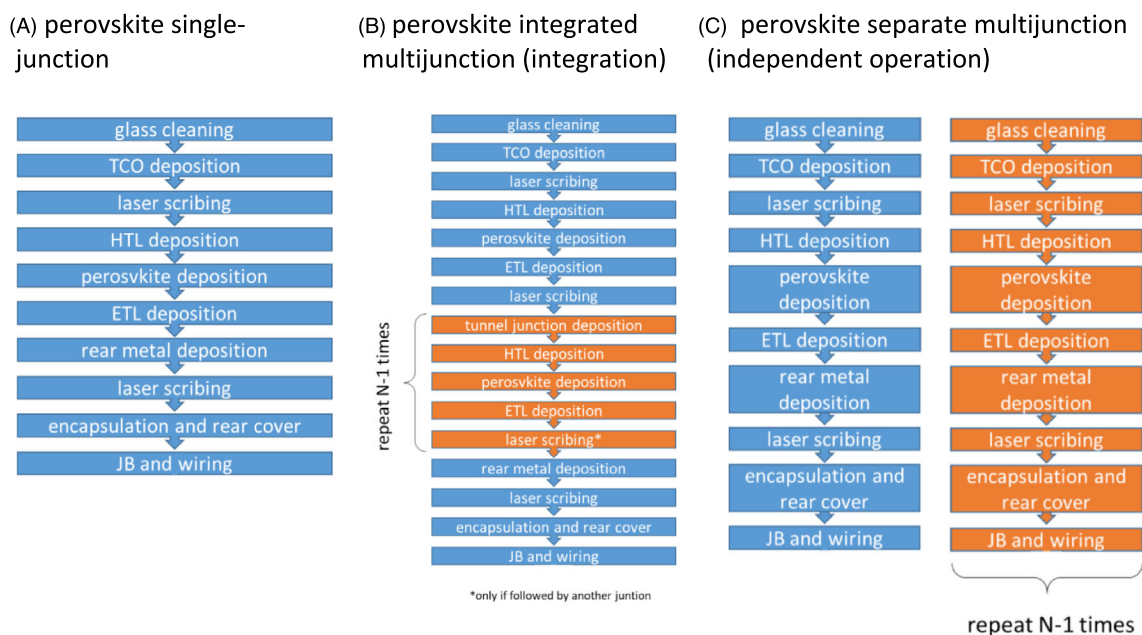
(A) perovskite single-junction

(B) perovskite integrated multijunction (integration)

(C) perovskite separate multijunction (independent operation)

FIGURE 6 Fabrication sequence used to model the cost of a single junction (A), monolithic multijunction (B) and spatially separated multijunction (C) solar cell. The process is based on the fabrication process of a perovskite solar cell published in Sofia et al.[35] The abbreviation TCO stands for transparent conductive oxide, HTL stands for hole transport layer, ETL for electron transport layer and JB stands for junction box.
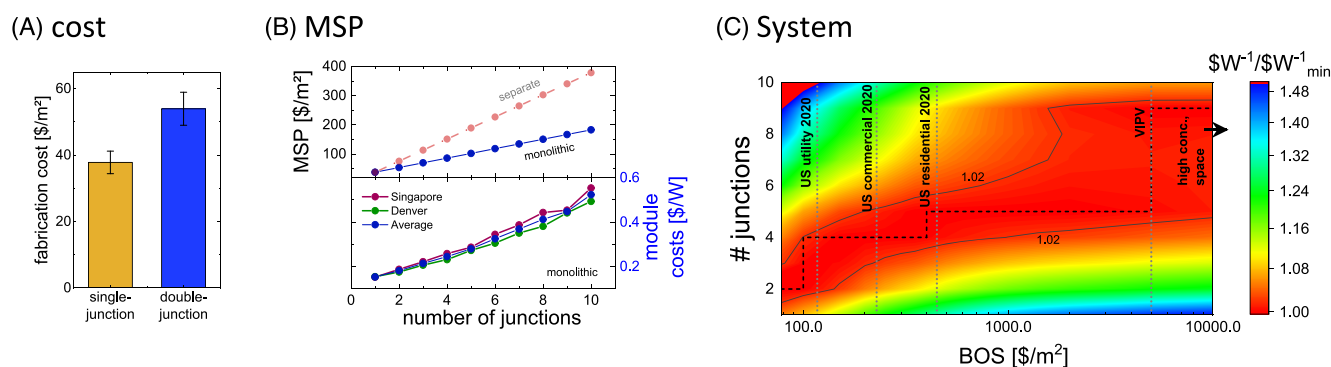
(A) cost **(B) MSP** **(C) System**

FIGURE 7 Techno-economic analysis of tandem solar cells. (A) Summary of literature data for the fabrication cost of a single-junction and a monolithically integrated double-junction perovskite solar cell. (B) Projected fabrication cost of a monolithic (blue) and separated (red) multijunction solar cell (bottom) and the calculated module cost per Watt with the assumption that modules operate at 75% of the detailed balance limit (top). (C) System cost as a function of BOS costs and costs normalized to the lowest value for each BOS cost. As BOS costs increase, efficiency gains in value and a greater number of junctions becomes attractive. The dashed line describes the discrete number of junctions with the lowest system costs; the solid lines mark the 2% range above the minimum in the corresponding 2D Kernel density.

Figure 6. Monolithic integration (Figure 6B) requires fewer additional steps and material compared to independent operation (Figure 6C), in which fabrication is doubled. The transition from 2 to N junctions is made by repeating the additional steps marked in brown. Note that we consider only solar cell fabrication here. System costs beyond cables as well as the optical elements needed for some concepts with independent cell operation are not included here. The reason we concentrate on cell fabrication is that a wide variety of possibilities exists for system integration that vary greatly in the corresponding cost.

Module integration in a voltage-matching configuration was shown to offer high yield at low cost, for example,[36] for double junction solar cells. Note that the calculation does not include optical elements needed for spectral distribution. As shown above, even elements with very good optical efficiency can generate notable losses. Generating optical elements of sufficient quality at low cost is a challenge for all concepts relying on them.

A literature search of cost numbers published between 2018 and 2022 for the fabrication of single-junction and tandem perovskite

solar cell suggests a minimum sustainable price of 38 ± 2 \$/m^2 for a perovskite single junction solar cell and 54 ± 3 \$/m^2 for a monolithically integrated double-junction solar cell (Figure 7A).[35,37–40] Note that we consider these to be aggressive cost targets for perovskite solar cells, given that silicon PV modules are at about 60 \$/m^2 and CdTe at 50 \$/m^2. In a simple model, we extrapolate the cost of a monolithically integrated multijunction solar cell to be $38 + (N-1) \cdot 16$ \$/m^2 and the cost of separately operated solar cells to be $N \cdot 38$ \$/m^2. The minimum sustainable price (MSP)[41] as a function of the number of junctions up to 10 is shown in Figure 7B on top. Note that for the subsequent calculations, we only use the numbers for monolithic integration. From MSP and efficiency, the \$/W$_P$ cost of a module can be calculated. These are shown in Figure 7B on the bottom for illumination without concentration. Fabrication costs outweigh efficiency increases, resulting in tandems with more junctions having a greater \$/W$_P$ cost, which is consistent with modelling for double junction solar cells.[42]

The true value of a tandem is only revealed in a system. Efficiency is the more valuable the higher balance of system (BOS) costs are. To give an impression of the economically ideal number of junctions, we calculate system costs as module costs + BOS costs (given in \$/m^2) as a function of the number of junctions and of BOS costs, and we normalize the result to the lowest system cost value for each BOS cost. The result of this calculation is shown in Figure 7C. The figure shows which number of junctions produces the lowest installed \$/W$_P$ cost for a range of applications. BOS costs for utility, commercial and residential installations in the United States were taken from Horowitz et al.[43] For vehicle integrated photovoltaics (VIPV), we used the costs for the, now discontinued, Sono Sion solar powered car, of 29.900 € (7 June 2022),[44] which has around 6 m^2 of solar cells integrated (resulting in "BOS" costs of 5000 €/m^2, though we agree of course that this approach is debatable). BOS costs for space applications were guessed. Space launches tend to be so expensive that efficiency improvement is worthwhile at costs much beyond the ones considered here. We observe that the economically ideal number of junctions increases slowly with BOS costs and remains below five up until BOS costs of 5000 \$/m^2. We also note that the minimum becomes broader; less than four junctions are sufficient to stay within 2% of the lowest system costs for the entire range of BOS costs covered.

While cost numbers for perovskite solar cells are necessarily hypothetical because commercial production is still in its infancy, commercial experience exists for III-V solar cells. Because manufacturing has concentrated on specialized markets like space applications and concentrator photovoltaics, published cost numbers vary, yet a few studies from NREL have looked into cost scenarios for mass-market applications. Published cost numbers for GanInP/GaAs and GaAS/Si double-junction solar cells are between 1300 and 1500 \$/m^2 at 30% efficiency with long-term prospects at 230 \$/m^2 at 35%.[45,46] The Sion is a cancelled electric car developed by Sono motors. The concept envisioned the integration of solar cells on all surfaces of the car. The project was cancelled in February 2023 (during the review process of this paper) as sufficient funding could not be secured. The last published cost estimate for the Sion was 29.900 €.[46] With these cost numbers, a meaningful estimate about the economically ideal number of junctions for given applications could not be made. For space or high-concentration applications, maximizing efficiency for any number of junctions appears to be a valid strategy.

8 | SUMMARY AND CONCLUSIONS

In this study, we explored how practical limitations affect the limiting efficiency and the ideal number of junctions in a tandem solar cell. For this purpose, we explored four tandem architectures based on optical considerations (Figure 1). Each of the shown architectures is capable of realizing highest efficiencies, yet each is affected by different principle loss mechanisms. In the absence of these losses, efficiencies monotonically increase with the number of junctions and approach the limit of the infinite tandem. Because some loss mechanisms affect a configuration with a greater number of junctions more than one with a smaller number, introducing them disrupts the monotonic increase and shifts the ideal number of junctions forward. One such loss mechanism is the variation of spectra for a series-connected tandem solar cell in outdoor operation. This variation results in current losses, as different junctions become limiting with varying spectrum. Calculations for 1 year in Singapore and Denver suggest that spectrum variations limit the achievable efficiency to below 75% (90% of the infinite tandem limit) and that no further harvesting efficiency improvements are possible after about nine junctions.

While independent cell operation is not affected by spectral variations in this way, the introduction of optical elements necessary for spectral selection and cell isolation induces a similar effect. Imperfections of the optical elements introduce losses that are greater for configurations with more junctions. How a non-ideal optical efficiency affects efficiency depends on the tandem architecture, yet in most cases, we find that an optical efficiency of 99% reduces the ideal number of junctions to below 10 and reduces achievable efficiencies by more than 10% compared to the infinite tandem limit.

For these results, we have assumed that the band gaps of all involved materials can be chosen freely. Yet for fundamental as well as for practical reasons, choices may not be entirely free. For III-V solar cell stacks, band gaps are typically between 0.6 eV and 2.45 eV; highly efficient perovskites can be varied between 1.24 eV and 2.3 eV. Exploring the impact of band gap limitations, we find that the availability of a low band-gap semiconductor with a band gap of 0.9 eV or below is expedient for realizing high efficiencies. Achievable efficiencies are more sensitive to low band gaps in the bottom cell than to high band gaps (above 2 eV) in the top cell. We note that a range between 0.9 eV and 2.5 eV is sufficient to approach configurations that are very close to the ideal ones, at least for up to six junctions.

A final limitation we explored is of economic nature. Introducing more junctions increases the cost for fabricating a tandem. Provided the utilized material is similar across junctions, a linear increase in cost

with numbers of junctions can be assumed. This linear increase stands against a diminishing efficiency increase for every new junction. At one point, this diminishing increase in efficiency will result in additional junctions becoming economically unfavourable. The position of this point depends on the balance of system costs associated for the tandem application. The greater these BOS costs are, the more efficiency is valuable,[47] and the more junctions are economically desirable. Looking at the example of an ideal all-perovskite tandem, we find that the economically ideal number of junctions is five are below for BOS costs up to 5000 \$/m^2. With a 2% margin, we find no situation, except maybe space applications, in which more than four junctions are needed.

AUTHOR CONTRIBUTIONS

ACKNOWLEDGEMENTS

DATA AVAILABILITY STATEMENT

The data that support the findings of this study are available in Spectral Solar Radiation Data Base at https://www.nrel.gov/grid/solar-resource/spectral-solar.html. These data were derived from the following resources available in the public domain: - Spectral Solar Radiation Data Base, https://www.nrel.gov/grid/solar-resource/spectral-solar.html.

ORCID

Carlos David Rodríguez Gallegos https://orcid.org/0000-0002-6755-3668

Larry Lüer https://orcid.org/0000-0001-9952-4207

REFERENCES

1. Würfel P. *Physics of Solar Cells: From Principles to New Concepts*. Wiley-VCH; 2005. doi:10.1002/9783527618545
2. De Vos A. Detailed balance limit of the efficiency of tandem solar cells. *J Phys D Appl Phys*. 1980;13(5):839-846. doi:10.1088/0022-3727/13/5/018
3. Shockley W, Queisser HJ. Detailed balance limit of efficiency of p-n junction solar cells. *J Appl Phys*. 1961;32(3):510-519. doi:10.1063/1.1736034
4. Geisz JF, Steiner MA, Jain N, et al. Building a six-junction inverted metamorphic concentrator solar cell. *IEEE J Photovolt*. 2018;8(2):626-632. doi:10.1109/JPHOTOV.2017.2778567
5. Fraunhofer ISE. Press Release #13 May 30th, 2022, Fraunhofer ISE Develops the World's Most Efficient Solar Cell with 47.6 Percent Efficiency.
6. France RM, Geisz JF, Song T, et al. Triple-junction solar cells with 39.5% terrestrial and 34.2% space efficiency enabled by thick quantum well superlattices. *Joule*. 2022;6(5):1121-1135. doi:10.1016/j.joule.2022.04.024
7. Bielawny A, Miclea PT, Rhein AV, Wehrspohn RB, Van Riesen S, Glunz S. Dispersive elements for spectrum splitting in solar cell applications, Proc. SPIE 6197, Photonics for Solar Energy Systems, 2006, 619704.
8. Yao Y, Liu H, Wua W. Fabrication of high-contrast gratings for a parallel spectrum splitting dispersive element in a concentrated photovoltaic system. *J Vac Sci Technol B*. 2014;32(6):06FG04. doi:10.1116/1.4898198
9. Barnett A, Kirkpatrick D, Honsberg C, et al. Very high efficiency solar cell modules. *Prog Photovolt: Res Appl*. 2009;17(1):75-83. doi:10.1002/pip.852
10. Chrysler BD, Shaheen SE, Kostuk RK. Lateral spectrum splitting system with perovskite photovoltaic cells. *J Photo Energy*. 2022;12(2):022206. doi:10.1117/1.JPE.12.022206
11. Darbe S, Escarra MD, Warmann EC, Atwater HA. Simulation and partial prototyping of an eight-junction holographic spectrum-splitting photovoltaic module. *Energy Sci Eng*. 2019;7(6):2572-2584. doi:10.1002/ese3.445
12. Goldschmidt JC, Peters M, Bösch A, et al. Increasing the efficiency of fluorescent concentrator systems. *Sol Energy Mater sol Cells*. 2009;93(2):176-182. doi:10.1016/j.solmat.2008.09.048
13. Ortabasi U. First experiences with a multi-band gap photovoltaic cavity converter (PVCC) module for ultimate solar-to-electricity conversion efficiency. In Proceedings of the 19th European Photovoltaic Solar Energy Conference, Paris, France, June 2004; 2256–2560.
14. Mitchell B, Peharz G, Siefer G, et al. Four-junction spectral beam-splitting photovoltaic receiver with high optical efficiency. *Prog Photovolt: Res Appl*. 2011;19(1):61-72. doi:10.1002/pip.988
15. Gouffé A. Corrections d'ouverture des corps-noirs artificiels compte tenu des diffusions multiples internes. *Revue d'Optique*. 1945; 24:1-3.
16. Onsager L. Reciprocal relations in irreversible processes. I. *Phys Rev*. 1931;37(4):405-426. doi:10.1103/PhysRev.37.405
17. Gueymard C, Myers D, Emery K. Proposed reference irradiance spectra for solar energy systems testing. *Solar Energy*. 2002;73(6):443-467.
18. Markvart T. Shockley: Queisser Detailed Balance Limit after 60 Years. *Wiley Interdisc Rev: Energy Environ*. 2022;11(4):e430. doi:10.1002/wene.430
19. King RR, Haddad M, Isshiki T, et al. Metamorphic GaInP/GaInAs/Ge solar cells, Proc. 28th IEEE PVSC, 15–22 Sept. 2000; 982–985.
20. Dimroth F, Schubert U, Bett AW. 25.5% efficient Ga0.35In0.65P/Ga0.83In0.17As tandem solar cells grown on GaAs substrates. *IEEE Electron Device Lett*. 2000;21(5):209-211. doi:10.1109/55.841298
21. Cariou R, Benick J, Feldmann F, et al. III–V-on-silicon solar cells reaching 33% photoconversion efficiency in two-terminal configuration. *Nat Energy*. 2018;3(4):326-333. doi:10.1038/s41560-018-0125-0
22. Bett A, Dimroth F, Stollwerck G, Sulima OV. III-V compounds for solar cell applications. *Appl Phys A*. 1999;69(2):119-129. doi:10.1007/s003390050983
23. Schuster O, Wientjes P, Shrestha S, et al. Looking beyond the surface: the band gap of bulk methylammonium lead iodide. *Nano Lett*. 2020; 20(5):3090-3097. doi:10.1021/acs.nanolett.9b05068

24. Noh JH, Im SH, Heo JH, Mandal TN, Seok SI. Chemical management for colorful, efficient, and stable inorganic−organic hybrid nanostructured solar cells. *Nano Lett*. 2013;13(4):1764-1769. doi:10.1021/nl400349b

25. Prasanna R, Gold-Parker A, Leijtens T, et al. Band gap tuning via lattice contraction and octahedral tilting in perovskite materials for photovoltaics. *J am Chem Soc*. 2017;139(32):11117-11124. doi:10.1021/jacs.7b04981

26. Pérez-López JJ, Fabero F, Chenlo F. Experimental solar spectral irradiance until 2500 nm: results and influence on the PV conversion of different materials. *Prog Photovolt: Res Appl*. 2007;15(4):303-315. doi:10.1002/pip.739

27. Gueymard CA. Parameterized transmittance model for direct beam and circumsolar spectral irradiance. *Solar Energy*. 2001;71: 325-346.

28. Faine P, Kurtz SR, Riordan C, Olson JM. The influence of spectral solar irradiance variations on the performance of selected single-junction and multijunction solar cells. *Solar Cells*. 1991;31(3):259-278. doi:10.1016/0379-6787(91)90027-M

29. Ripalda JM, Buencuerpo J, García I. Solar cell designs by maximizing energy production based on machine learning clustering of spectral variations. *Nat Commun*. 2018;9(1):5126. doi:10.1038/s41467-018-07431-3

30. Liu H, Aberle AG, Buonassisi T, Peters IM. On the methodology of energy yield assessment for one-Sun tandem solar cells. *Solar Energy*. 2016;135:598-604. doi:10.1016/j.solener.2016.06.028

31. Hörantner MT, Snaith HJ. Predicting and optimising the energy yield of perovskite-on-silicon tandem solar cells under real world conditions. *Energ Environ Sci*. 2017;10(9):1983-1993. doi:10.1039/C7EE01232B

32. Peters IM, Liu H, Reindl T, Buonassisi T. Global prediction of photovoltaic field performance differences using open-source satellite data. *Joule*. 2018;2(2):307-322. doi:10.1016/j.joule.2017.11.012

33. Andreas A, Stoffel T. NREL Solar Radiation Research Laboratory (SRRL): baseline measurement system. NREL Report No DA5500-56488, Golden, Colorado; 1981.

34. Liu H, Ren Z, Liu Z, Aberle AG, Buonassisi T, Peters IM. Predicting the outdoor performance of flat-plate III–V/Si tandem solar cells. *Solar Energy*. 2017;149:77-84. doi:10.1016/j.solener.2017.04.003

35. Sofia SE, Wang H, Bruno A, Cruz-Campa JL, Buonassisi T, Peters IM. Roadmap for cost-effective, commercially-viable perovskite silicon tandems for the current and future PV market. *Sustain Energy Fuel*. 2020;4(2):852-862. doi:10.1039/C9SE00948E

36. Liu H, Rodríguez-Gallegos CD, Liu Z, Buonassisi T, Reindl T, Peters IM. A worldwide theoretical comparison of outdoor potential for various silicon-based tandem module architecture. *Cell Rep Phys Sci*. 2020;1(4):100037. doi:10.1016/j.xcrp.2020.100037

37. Song Z, Phillips AB, Celik I et al. Manufacturing cost analysis of perovskite solar modules in single-junction and all-perovskite tandem configurations, 2018 IEEE 7th World Conference on Photovoltaic Energy Conversion (WCPEC) (A Joint Conference of 45th IEEE PVSC, 28th PVSEC & 34th EU PVSEC), Waikoloa, HI, USA, 2018; 1134–1138, doi:10.1109/PVSC.2018.8547676.

38. Messmer C, Goraya BS, Nold S, et al. The race for the best silicon bottom cell: efficiency and cost evaluation of perovskite–silicon tandem solar cells. *Prog Photovolt Res Appl*. 2021;29(7):744-759. doi:10.1002/pip.3372

39. Moot T, Werner J, Eperon GE, et al. Choose your own adventure: fabrication of monolithic all-perovskite tandem photovoltaics. *Adv Mater*. 2020;32(50):2003312. doi:10.1002/adma.202003312

40. Li Z, Zhao Y, Wang X, et al. Cost analysis of perovskite tandem photovoltaics. *Joule*. 2018;2(8):1559-1572. doi:10.1016/j.joule.2018.05.001

41. Powell DM, Winkler MT, Goodrich A, Buonassisi T. Modeling the cost and minimum sustainable price of crystalline silicon photovoltaic manufacturing in the United States. *IEEE J Photovolt*. 2013;3(2): 662-668. doi:10.1109/JPHOTOV.2012.2230056

42. Sofia SE, Mailoa JP, Weiss DN, Stanbery BJ, Buonassisi T, Peters IM. Economic viability of thin-film tandem solar modules in the United States. *Nat Energy*. 2018;3(5):387-394. doi:10.1038/s41560-018-0126-z

43. Horowitz KAW, Remo T, Smith B, Ptak A. *Techno-Economic Analysis and Cost Reduction Roadmap for III-V Solar Cells*. National Renewable Energy Laboratory; 2018. NREL/TP-6A20-72103. https://www.nrel.gov/docs/fy19osti/72103.pdf

44. Essig S, Allebé C, Remo T, et al. Raising the one-sun conversion efficiency of III–V/Si solar cells to 32.8% for two junctions and 35.9% for three junctions. *Nat Energy*. 2017;2(9):17144. doi:10.1038/nenergy.2017.144

45. Feldman D, Ramasamy V, Fu R, Ramdas A, Desai J, Margolis R. *U.S. Solar Photovoltaic System Cost Benchmark: Q1 2020*. National Renewable Energy Laboratory; 2021. NREL/TP-6A20-77324.

46. https://en.wikipedia.org/wiki/Sono_Motors_Sion.

47. Peters IM, Rodriguez Gallegos CD, Sofia SE, Buonassisi T. The value of efficiency in photovoltaics. *Joule*. 2019;3(11):2732-2747. doi:10.1016/j.joule.2019.07.028

SUPPORTING INFORMATION

Additional supporting information can be found online in the Supporting Information section at the end of this article.